Power and Life Extension of Battery–Ultracapacitor Hybrids

R. A. Dougal, *Senior Member, IEEE*, Shengyi Liu, *Member, IEEE*, and Ralph E. White

***Abstract*—The performance of a battery–ultracapacitor hybrid power source under pulsed load conditions is analytically described using simplified models. We show that peak power can be greatly enhanced, internal losses can be considerably reduced, and that discharge life of the battery is extended. Greatest benefits are seen when the load pulse rate is higher than the system eigen-frequency and when the pulse duty is small. Actual benefits are substantial; adding a 23 F ultracapacitor bank (3×7 PC10 ultracapacitors) in parallel with a typical Li-ion battery of 7.2 V and 1.35 A hr capacity can boost the peak power capacity by 5 times and reduce the power loss by 74%, while minimally impacting system volume and weight, for pulsed loads of 5 A, 1 Hz repetition rate, and 10% duty.**

***Index Terms*—Battery–ultracapacitor hybrids, life-cycle extension, optimization design.**

I. Nomenclature

C_c	Nominal capacitance of an ultracapacitor cell (F).
D	Pulse duty ratio.
f	Pulse frequency (Hz).
$I_{b,\mathrm{peak}}$	Battery peak current (A).
$I_{b,\mathrm{rms}}$	Battery root-mean-square current (A).
i_b	Battery current (A).
$i_{b,\mathrm{ss}}$	Steady state battery current (A).
$I_{c,\mathrm{rms}}$	Capacitor root-mean-square current (A).
i_c	Ultracapacitor current (A).
$i_{c,\mathrm{ss}}$	Steady state ultracapacitor current (A).
I_L	Average load current (A).
I_o	Amplitude of the output current (A).
$I_o(s)$	Frequency domain output current.
$I_{o,\mathrm{rms}}$	Root-mean-square of the output current (A).
i_o	Output current (A).
I_{rated}	Battery rated current (A).
m	Ultracapacitor bank configuration number.
N	Number of pulses to discharge the battery.
n_b	Number of battery cells.
n_p	Number of ultracapacitor cells in parallel.
n_s	Number of ultracapacitor cells in series.
R_b	Internal resistance of the battery cell (Ω).
R_c	Internal resistance of the ultracapacitor cell (Ω).
$P_{i,b}$	Power loss in the battery (W).
$P_{i,\mathrm{bc}}$	Battery–ultracapacitor hybrid power loss (W).
P_o	Output power (W).
P_{peak}	Battery peak power (W).
P_{rated}	Battery rated power (W).
s	Complex frequency.
t	Time (s).
T	Period of the pulsed current (s).
V_b	Open-circuit voltage of the battery (V).
V_{bo}	Output voltage for battery-only system (V).
V_{c0}	Initial voltage of capacitor (V).
V_i	Frequency domain internal voltage drop.
V_{Th}	Frequency domain Thevenin equivalent voltage source.
v_i	Internal voltage drop (V).
v_o	Output voltage (V).
v_{Th}	Thevenin equivalent voltage source (V).
W_i	Energy loss in the battery (J).
$W_{i,\mathrm{bc}}$	Battery–ultracapacitor energy loss (J).
W_T	Total energy stored in the battery (J).
ΔW	Energy saved with battery–ultracapacitor system (J).
Z_{Th}	Frequency domain Thevenin equivalent impedance.
z_{Th}	Thevenin equivalent impedance (Ω).
α	Capacitor eigen-frequency (Hz).
β	System eigen-frequency (Hz).
δ	Ratio of output current to the battery short-circuit current.
$\Phi(t)$	Unit step function.
γ	Power enhancement factor.
ε	Power saving factor.
λ	Ratio of the battery rms current to the load rms current.
μ	Ratio of the capacitor rms current to the load rms current.
τ_{bo}	Battery discharge cycle time (s).
τ_{bc}	Battery–ultracapacitor system discharge cycle time (s).
$\Delta\tau$	Battery discharge time extension (s).
ζ	Ultracapacitor current partition.

Manuscript received June 12, 2001; revised November 14, 2001. This work was supported by the U.S. Army Communications and Electronics Command under Contract (NRO-00-C-0134). This work was recommended for publication by Associate Editor M. Swaminathan upon evaluation of the reviewers' comments.

The authors are with the College of Engineering, University of South Carolina, Columbia, SC 29208 USA (e-mail: lius@engr.sc.edu).

Publisher Item Identifier S 1521-3331(02)02308-5.

II. Introduction

ULTRACAPACITORS (or electrochemical double layer capacitors, supercapacitors [1]–[4]) are increasingly interesting because of their high-energy density (compared to conventional capacitors) and high-power density (compared to batteries and fuel cells). Reports of ultracapacitor applications in power distribution systems [5], [6] and in utility electronic apparatus [7]–[9] have described improvements in power quality, uninterrupted power supply (UPS), and memory backup. Considerable efforts [10]–[14] have been invested to exploit the

high-power capability of ultracapacitor hybrids with batteries or fuel cells in pulsed operating modes, which are of particular interest to portable power systems, electric vehicles and digital telecommunication systems. Advanced battery technologies now allow extraordinary energy densities, but often insufficient power densities for applications where the load draws large power impulses. This deficiency can be overcome by paralleling more batteries if that is allowed by system volume, weight, and cost constraints. On the other hand, parallel hybrid power sources that combine advanced batteries with ultracapacitors can overcome the power deficiency at lower monetary, volumetric, or weight cost. Such systems have been experimentally demonstrated longer operating times [10], [11], [13] compared to systems without ultracapacitors. However, the literature is deficient in theoretical analysis of such systems with respect to energy efficiency, power capabilities and cost effectiveness. It is of practical importance for engineers to have some reasonable theoretical basis to achieve optimized system designs. The present paper is intended to fill out that void by providing a method and analytic results for a simplified model of the battery–ultracapacitor system operating under pulsed conditions. The analysis focuses on the interrelations between battery, ultracapacitor and load in terms of their power and energy partitions, so that the potential gains in peak power, reduction of internal losses and extension of discharge life can be revealed and evaluated.

III. Circuit Model

A. Circuit Description

The basic circuit considered in this analysis is shown in Fig. 1(a) and its Thevenin equivalent in frequency domain in Fig. 1(b). The models used here are greatly simplified for the sake of making the analysis tractable. (A much more complex model of the system is studied in a follow-on paper using computational analysis.) The ultracapacitor is modeled by a nominal capacitance C_c and an equivalent series resistance R_c, and the battery by an ideal voltage source V_b and an internal resistance R_b. The battery has a certain capacity in terms of moles of reactive material and therefore coulombs of stored charge. For the purposes of this analysis, the capacity is assumed to be rate independent. (Actually, the capacity of a battery *is* rate dependent and performance improvements obtained should therefore be better than presented in this analysis.) The electric power available at the external terminals depends on internal losses which are caused mainly by internal resistance. In this paper, we characterize that as a very simple, single, lumped equivalent series resistance. Similarly, the capacitor actually has a very complex charge/discharge characteristic having multiple time constants [2], [3], [10], or more specifically, having distributed capacitance and resistance. Yet, for the purposes of this analysis, we will characterize it as a single lumped capacitance and a single lumped resistance, as it appeared in [8]. It is expected that the analytical results based on the simplified model will deviate from the actual performance at high frequencies (>kHz) at which the stray inductance (∼nH, [2], [10]) and the distributed capacitance nature of both ultracapacitor and battery dominate. However, operations of frequencies higher than kHz are beyond the present scope of battery/ultracapacitor hybrid scheme. Within the range of pulse rates from 0.01 to 10 Hz, our separate simulation study using a more complicated ladder model [2], [10] indicates that the simplified model can well represent the primary features of ultracapacitor. In addition, the simplified model allows to infer significant conclusions without introducing unnecessary complications, as will be detailed in this and subsequent sections.

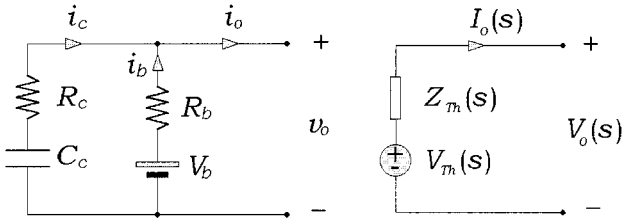

Fig. 1. Circuit of an ultracapacitor in parallel with a battery, and its Thevenin equivalent in frequency domain.

The Thevenin equivalent voltage and impedance of the parallel system in the frequency domain [shown in Fig. 1(b)] are described by

$$V_{\rm Th}(s) = \frac{R_c}{R_b + R_c} V_b \frac{s+\alpha}{s(s+\beta)} + \frac{R_b}{R_b + R_c} V_{c0} \frac{1}{s+\beta} \quad (1)$$

$$Z_{\rm Th}(s) = \frac{R_b R_c}{R_b + R_c} \frac{s+\alpha}{s+\beta} \quad (2)$$

where s is the complex frequency, V_{c0} is the initial voltage of the ultracapacitor, and

$$\alpha = \frac{1}{R_c C_c} \quad (3)$$

$$\beta = \frac{1}{(R_b + R_c) C_c}. \quad (4)$$

Now, assuming a pulsed load current with pulse frequency f (the period $T = 1/f$) and pulse duty ratio D, the current for the first N pulses can be expressed as

$$i_o(t) = I_o \cdot \sum_{k=0}^{N-1} [\Phi(t - kT) - \Phi(t - (k+D)T)] \quad (5)$$

where I_o is the amplitude of the current and $\Phi(t)$ is a unit step function at $t = 0$. The current in frequency domain can be found by performing the Laplace transform operation on (5), yielding the result

$$I_o(s) = I_o \sum_{k=0}^{N-1} \left[\frac{e^{-kT \cdot s}}{s} - \frac{e^{-(k+D)T \cdot s}}{s} \right]. \quad (6)$$

The average value of the load current can be expressed as the product of the pulsed amplitude times the duty factor D as

$$I_L = D I_o. \quad (7)$$

B. Solution

The output voltage is a linear combination of the Thevenin voltage source and the internal voltage drop. The inverse Laplace transform of the Thevenin voltage source, according to (1), is

$$v_{\rm Th}(t) = V_b + \frac{R_b}{R_b + R_c} (V_{c0} - V_b) e^{-\beta \cdot t}. \quad (8)$$

The second term of (8) is due to the energy redistribution between the ultracapacitor and the battery at the beginning of the discharge. When $t \to \infty$, $v_{\rm Th}(t) = V_b$.

For the current waveform defined by (5), the internal voltage drop $V_i(s)$ is

$$\begin{aligned} V_i(s) =& Z_{\rm Th} I_o(s) \\ =& \frac{R_b R_c}{R_b + R_c} I_o \sum_{k=0}^{N-1} \left[\left(\frac{\alpha}{\beta} \frac{1}{s} + \frac{\beta - \alpha}{\beta} \frac{1}{s+\beta} \right) \right. \\ & \left. \times \left(e^{-kT \cdot s} - e^{-(k+D)T \cdot s} \right) \right]. \end{aligned} \tag{9}$$

The corresponding expression in the time domain is

$$\begin{aligned} v_i(t) =& R_b I_o \\ & \times \sum_{k=0}^{N-1} \left[\left(1 - \frac{R_b}{R_b + R_c} e^{-\beta(t-kT)} \right) \Phi(t - kT) \right. \\ & - \left(1 - \frac{R_b}{R_b + R_c} e^{-\beta[t-(k+D)T]} \right) \\ & \left. \times \Phi[t - (k+D)T] \right]. \end{aligned} \tag{10}$$

From the circuit shown in Fig. 1, the output voltage can be found as

$$V_o(s) = V_{\rm Th}(s) - V_i(s). \tag{11}$$

Applying the linear property of the Laplace transform to (11) and using (8) and (10), one obtains

$$\begin{aligned} v_o(t) =& v_{\rm Th}(t) - v_i(t) \\ =& V_b + \frac{R_b}{R_b + R_c} (V_{c0} - V_b) e^{-\beta \cdot t} \\ & - R_b I_o \sum_{k=0}^{N-1} \left[\left(1 - \frac{R_b}{R_b + R_c} e^{-\beta(t-kT)} \right) \Phi(t - kT) \right. \\ & - \left(1 - \frac{R_b}{R_b + R_c} e^{-\beta[t-(k+D)T]} \right) \\ & \left. \times \Phi[t - (k+D)T] \right]. \end{aligned} \tag{12}$$

The currents from the battery and the ultracapacitor can be found once the output voltage is resolved. These currents are

$$i_b(t) = \frac{1}{R_b} [V_b - v_o(t)] \tag{13}$$

$$i_c(t) = i_o(t) - i_b(t). \tag{14}$$

The normalized load current (dotted), battery current (solid) and ultracapacitor current (dashed) as described by (5), (13), and (14), respectively, are plotted in Fig. 2 for the particular case $C_c = 20$ F, $R_c = 0.025\ \Omega$, and $R_b = 0.15\ \Omega$, pulse frequency 0.1 Hz, and load duty 0.1. Observe that both the battery and the ultracapacitor supply currents to the load during the load on-state, while, the battery charges the ultracapacitor during the load off-state. The instantaneous battery current, which otherwise would be the same level as the output current, is reduced considerably due to the assistance of the ultracapacitor.

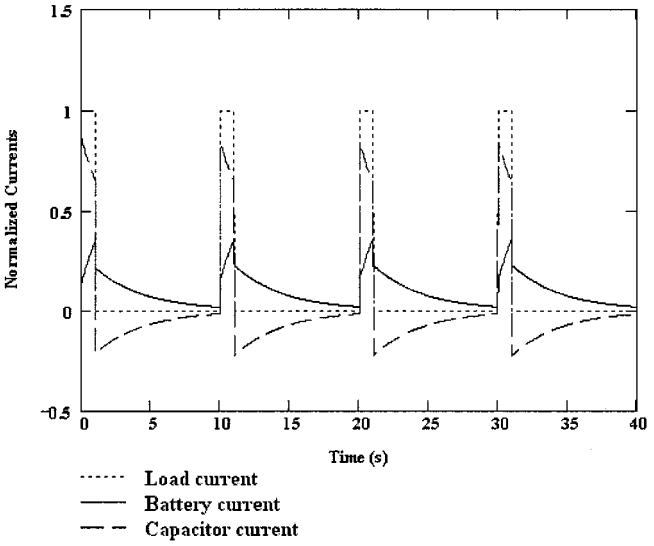

Fig. 2. Normalized currents (the dotted for the load current; the solid for the battery current and the dashed for the ultracapacitor current) for $f = 0.1$ Hz, $D = 0.1$.

The current supplied by the ultracapacitor during the load on-state relieves peak stresses on the battery and therefore positively influences the system performance. The percentage of the current supplied by the capacitor depends not only on the capacitor bank size and configuration, but also on the operating conditions such as the pulse rate and duty ratio. The effect of these factors on system performances is presented next.

IV. Performance Analysis

Let us focus on steady state operation of the battery–ultracapacitor system in this pulsed mode. Under scrutiny is the peak power enhancement, the internal loss reduction and the total run time extension. For pulsed loads, both battery temperature and peak currents can be reduced by using the ultracapacitor. To simplify the analysis we assume that the battery has an ideal rectangular amp-hour characteristic and a unit amp-hour capacity, as shown in Fig. 3. In reality, the open circuit voltage generally decreases as the battery is depleted and the battery current must be limited to protect the battery from degradation caused by excessive heating. Here, we consider times long compared to the time for energy redistribution between the battery and the ultracapacitor. Note that the time constant of the battery–ultracapacitor system [given by the reciprocal of (4)] is usually in seconds, while the discharge life of the battery is in hours.

Equations (12) and (13) yield the steady state battery current as

$$\begin{aligned} i_{b,\rm ss}(t) =& \frac{1}{R_b} v_i(t) \\ =& I_o \sum_{k=0}^{N-1} \left[\left(1 - \frac{R_b}{R_b + R_c} e^{-\beta(t-kT)} \right) \Phi(t - kT) \right. \\ & - \left(1 - \frac{R_b}{R_b + R_c} e^{-\beta[t-(k+D)T]} \right) \\ & \left. \times \Phi[t - (k+D)T] \right]. \end{aligned} \tag{15}$$

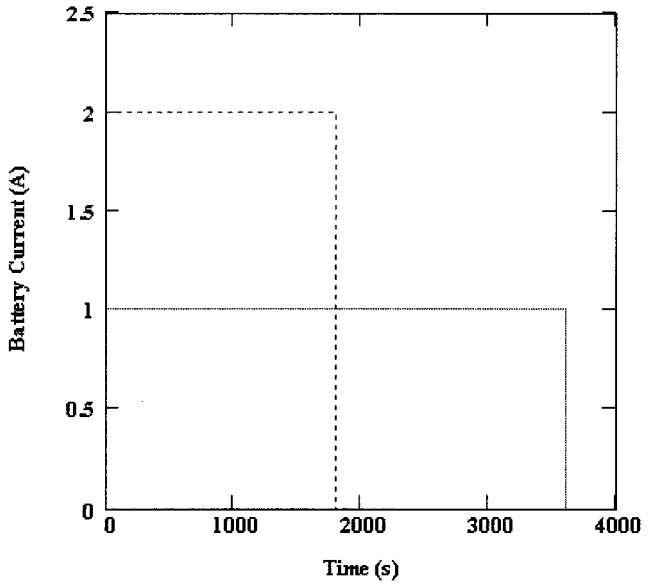

Fig. 3. Ideal amp-hour characteristics of batteries. The capacity of the battery is 1 A h. At a current of 2 A, the total discharge time will be 30 min (dotted).

Similarly, from (14), the steady state ultracapacitor current is

$$i_{c,\mathrm{ss}}(t) = \frac{R_b I_o}{R_b + R_c} \sum_{k=0}^{N-1} \Big[e^{-\beta(t-kT)} \Phi(t - kT) - e^{-\beta[t-(k+D)T]} \Phi\left[t - (k+D)T\right] \Big]. \quad (16)$$

A. Peak Power Enhancement

With the assistance of the ultracapacitor bank, Fig. 2 shows that the peak battery current is reduced to a fraction of the peak output current. This leads to reduction of the internal voltage drop in the battery. It can be reasonably assumed that the output voltage is nearly a constant. The peak power of the battery is therefore coincident with the peak current. Equation (15) predicts, and Fig. 2 shows, that the maximum battery current occurs at $t = (k+D)T$. The magnitude of the peak current during steady state pulse operation, according to (15) is (see derivation in the Appendix)

$$\begin{aligned} I_{b,\mathrm{peak}} &= I_o \left(1 - \frac{R_b e^{-\beta DT}}{R_b + R_c} \frac{1 - e^{-\beta(1-D)T}}{1 - e^{-\beta T}} \right) \\ &= I_o \left(1 - \zeta_c\right) = \frac{I_o}{\gamma} \end{aligned} \quad (17)$$

where

$$\zeta_c = \frac{R_b}{R_b + R_c} \frac{e^{-\beta DT} \left(1 - e^{-\beta(1-D)T}\right)}{1 - e^{-\beta T}} \quad (18)$$

is the capacitor current sharing factor at the peak power point, and

$$\gamma = \frac{1}{1 - \zeta_c} = \frac{1}{1 - \frac{R_b}{R_b + R_c} \frac{e^{-\beta DT}\left(1 - e^{-\beta(1-D)T}\right)}{1 - e^{-\beta T}}}. \quad (19)$$

If I_{rated} is the rated current of the battery—i.e., the current at which the battery will have a normal discharge life as specified by the manufacturer's data sheet, then the magnitude of the output current of the battery–ultracapacitor system in terms of the rated current is

$$I_o = \gamma \cdot I_{\mathrm{rated}}. \quad (20)$$

The instantaneous peak power at rated current is

$$P_{\mathrm{peak}} = I_o V_b = \gamma \cdot I_{\mathrm{rated}} V_b = \gamma \cdot P_{\mathrm{rated}} \quad (21)$$

where P_{rated} is the rated power of the battery.

Since γ is larger than 1, (21) indicates that the peak output power of the battery–ultracapacitor hybrid is enhanced by a factor of γ which we call the power enhancement factor of the system. Fig. 4 shows how the power enhancement factor varies with pulse duty and pulse frequency. The frequency is normalized to the system eigen-frequency given by (4), which is of a value 0.286 Hz if the device parameter values $C_c = 20$ F, $R_c = 0.025\ \Omega$, and $R_b = 0.15\ \Omega$ are used. For all frequencies calculated, the factor increases as the pulse duty decreases, and as $D \to 0$, it approaches a value determined by the resistance of the capacitor and the battery, as given by

$$\gamma \to \frac{R_b + R_c}{R_c}. \quad (22)$$

Equation (22) is the maximum peak power enhancement factor that can possibly be achieved with a single cell ultracapacitor; in this example it has value 7.0. It is obviously advantageous to choose capacitors with small series resistance. At a given duty, the peak power enhancement increases with pulse frequency. For example, at $D = 0.2$, the power enhancement factor is 1 (no enhancement) at a pulse frequency of 0.01β Hz. The power enhancement factor is 1.13 for 0.1β Hz, 2.6 for 1.0β Hz and 3.1 for 10β Hz. When the operating frequency is higher than the system eigen-frequency [(4)], the enhancement factor approaches the

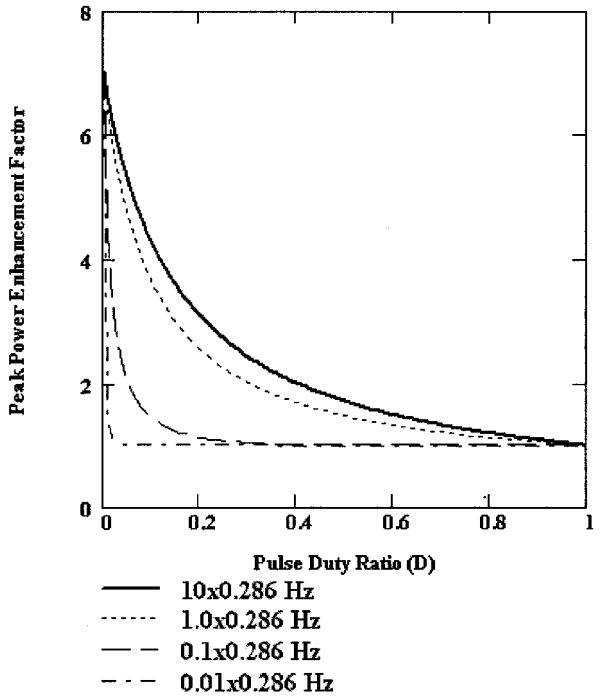

Fig. 4. Peak power enhancement factor as a function of the pulse duty ratio for different pulse frequencies. The ultracapacitor bank configuration index $m = 1$.

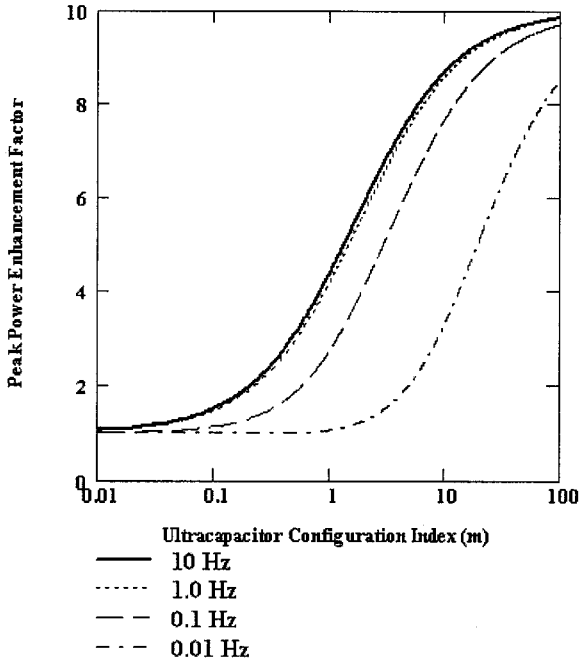

Fig. 5. Power enhancement as a function of the ultracapacitor bank configuration index number for different pulse frequencies. $D = 0.1$.

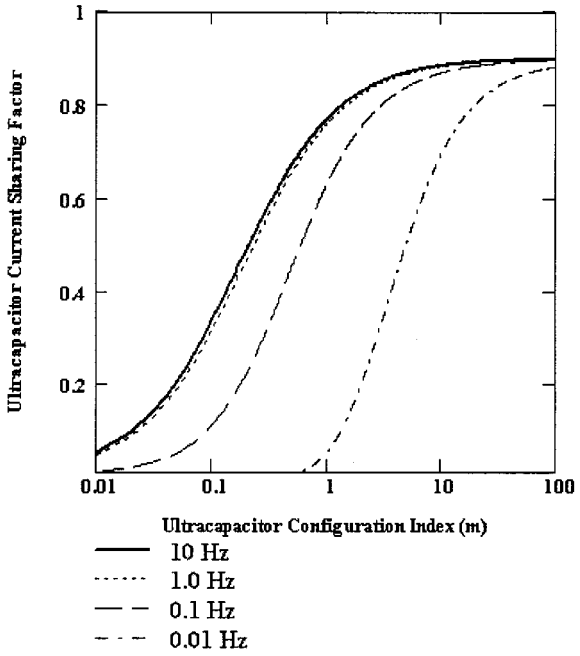

Fig. 6. Ultracapacitor current sharing factor as a function of configuration index for different pulse frequencies. $D = 0.1$.

limit (the thick line). In this case, the line for 10β Hz is already in the limit.

Increasing the capacitance by paralleling ultracapacitors decreases the equivalent series resistance of the bank while increasing the voltage rating by series connections increases the resistance. Defining n_p as the number of parallel capacitors and n_s as the number of series capacitors, we then define a configuration index m that characterizes the capacitor bank configuration as

$$m = \frac{n_p}{n_s}. \tag{23}$$

Note that $m > 1$ when there are more parallel connections than series connections, and $m < 1$ otherwise. For convenience in the discussion, we allow m to assume any real value larger than zero, though obviously in practice n_p and n_s must be discrete.

Now (4) can be rewritten as

$$\beta(m) = \frac{1}{\left(R_b + \frac{R_c}{m}\right) \cdot mC_c}. \tag{24}$$

Obviously, increasing m will reduce the system eigen-frequency. Since the power enhancement is most effective at pulse rates larger than the eigen-frequency, (24) implies that the increasing m can broaden the range of frequencies over which power enhancement can be achieved. The peak power enhancement factor as a function of m is

$$\gamma(m) = \frac{1}{1 - \frac{R_b e^{-\beta(m)DT}}{R_b + \frac{R_c}{m}} \frac{1 - e^{-\beta(m)(1-D)T}}{1 - e^{-\beta(m)T}}}. \tag{25}$$

Equation (25) is graphed in Fig. 5 for 10 Hz (solid), 1 Hz (dotted), 0.1 Hz (dashed) and 0.01 Hz (dot-dashed), all at pulse duty $D = 0.1$. The peak power monotonically increases as m increases (more parallel connections). Notice that the system eigen-frequency decreases as m increases. The maximum eigen-frequency is obtained when m is very small, and it is $\beta_{\max} = 1/(R_c C_c) = 2$ Hz in this case. Therefore the enhancement for operating frequencies higher than 2 Hz approaches the limit. This is shown by the thicker line in Fig. 5 that corresponds to 10 Hz ($>$2 Hz). Physically, the maximum eigen-frequency corresponds to the configuration of a single string of capacitors in series. For any configurations of several parallel strings, the system eigen-frequency is reduced. The available power enhancement increases as the eigen-frequency decreases (or the index number m increases). However, the enhancement for operations at frequencies higher than 2 Hz can be no more than that at 2 Hz for all configurations unless the internal resistance of the ultracapacitors is reduced. This fact can be taken into consideration in the practical design of a battery/ultracapacitor system to determine its best operating frequency range.

Examining Fig. 5, it seems that, when m is very large, a limit to power enhancement exists for all frequencies. Indeed, the limit exists and can be found from (25). It is given by (26).

$$\gamma \underset{m \to \infty}{\to} \frac{1}{D}. \tag{26}$$

For $D = 0.1$, the maximum peak power enhancement factor that can be achieved is 10. Accordingly, the pulse duty ratio is preferred to be small for power enhancement.

The enhancement of the instantaneous peak power capacity is due to the high power capacity of the ultracapacitor bank that, during the load-on state, shares a large part of the total load current. The fraction of the current shared by the capacitor bank as a function of m, at the maximum power point, is given by

$$\zeta_c(m) = \frac{R_b e^{-\beta(m)DT}}{R_b + \frac{R_c}{m}} \frac{1 - e^{-\beta(m)(1-D)T}}{1 - e^{-\beta(m)T}} \tag{27}$$

which is graphically shown in Fig. 6. Obviously, for a single cell ultracapacitor ($m = 1$), a smaller series resistance gives rise to higher current sharing. For a capacitor bank, increasing m number decreases the total series resistance, which increases the

current sharing. Also, higher pulse frequencies result in larger current sharing. When the operating frequency is much higher than the maximum eigen-frequency (2 Hz) of the battery–ultracapacitor system, the sharing factor approaches the limit (shown in Fig. 6 by the thicker line). Also, increasing m to a large value will obtain a maximum current sharing factor for all frequencies. This can be found as

$$\zeta_c \underset{m\to\infty}{\to} (1-D) \tag{28}$$

which yields 0.9 for $D = 0.1$. Because the peak power enhancement is a direct result of the current sharing by the ultracapacitor, both (25) and (27) play the same role in the design optimization.

B. Internal Loss Reduction

The internal losses during each cycle are reduced because a large part of the output current flows through the capacitor which has a smaller resistance, thereby leading to lower heating of the battery. To see this, we first look at the total energy W_b that can be delivered by the battery without the assistance of the ultracapacitor. If a pulsed current given by (5) is drawn from the battery, then

$$\begin{aligned} W_b &= \left(V_b\sqrt{D}I_o - R_b D I_o^2\right)\cdot\tau_{\rm bo} \\ &= V_b\sqrt{D}I_o\left(1-\frac{R_b\sqrt{D}I_o}{V_b}\right)\cdot\tau_{\rm bo} \\ &= V_{\rm bo}I_{o,\rm rms}\tau_{\rm bo} \end{aligned} \tag{29}$$

where $\tau_{\rm bo}$ is the total discharge time, $V_{\rm bo}$ is the battery output voltage and $I_{o,\rm rms}$ is the root-mean-square (rms) current flowing through the battery. The voltage and current are given by (30) and (31), respectively

$$V_{\rm bo} = V_b(1-\delta\sqrt{D}) \tag{30}$$

$$I_{o,\rm rms} = \sqrt{D}I_o. \tag{31}$$

δ is the ratio of the amplitude of the load current to the battery short-circuit current given by

$$\delta = \frac{R_b I_o}{V_b}. \tag{32}$$

Because ideal amp-hour characteristics are assumed in this analysis (see Fig. 3), we can run the battery to 100% depth of discharge. The internal energy loss in this case is

$$W_i = R_b I_{o,\rm rms}^2\tau_{\rm bo} = R_b D I_o^2\tau_{\rm bo}. \tag{33}$$

Now consider the battery to be connected to the circuit as shown in Fig. 1, while the load draws a pulsed output current also given by (5). To find the total energy lost inside the hybrid power source we calculate the root-mean-square currents from both the battery and the ultracapacitor. Consider first the nth pulse of the battery current, which can be derived from (15) as

$$\begin{aligned} i_{b,\rm ss}^{n\rm th}(t) = I_o\Bigg\{\sum_{k=0}^{n}\Bigg[&\left(1-\frac{R_b}{R_b+R_c}e^{-\beta(t-kT)}\right)\Phi(t-kT) \\ &-\left(1-\frac{R_b}{R_b+R_c}e^{-\beta[t-(k+D)T]}\right) \\ &\times\Phi\left[t-(k+D)T\right]\Bigg]\Bigg\} \\ &\times\left\{\Phi(t-nT)-\Phi[t-(n+1)T]\right\}. \end{aligned} \tag{34}$$

Since the steady state is considered, the nth pulse in (34) is a representation of pulses in the pulse train. The rms value of the battery current is then calculated as (see Appendix) (35), shown at the bottom of the page, where λ stands for the factor of the square root in (35). Similarly, the nth pulse for the ultracapacitor current in (16) is

$$\begin{aligned} i_{c,\rm ss}^{n\rm th}(t) = \frac{R_b I_o}{R_b+R_c}\Bigg\{\sum_{k=0}^{n}\Big[&e^{-\beta(t-kT)}\Phi\left(t-kT\right) \\ &-e^{-\beta[t-(k+D)T]}\Phi\left[t-(k+D)T\right]\Big]\Bigg\} \\ &\times\left\{\Phi(t-nT)-\Phi[t-(n+1)T]\right\}. \end{aligned} \tag{36}$$

And the rms value of the ultracapacitor current is (37), shown at the bottom of the page, where μ stands for the factor of the

$$\begin{aligned} I_{b,\rm rms} &= \sqrt{\frac{1}{T}\int_{nT}^{(n+1)T}\left[i_{b,\rm ss}^{n\rm th}\right]^2 dt} \\ &= \sqrt{D}I_o\sqrt{1+\frac{R_b}{R_b+R_c}\frac{2\left(1-e^{-\beta DT}\right)}{\beta DT}\left(\frac{1-e^{-\beta DT}}{1-e^{\beta T}}-1\right)+\left(\frac{R_b}{R_b+R_c}\right)^2\frac{\left(e^{\beta DT}-1\right)\left(1-e^{\beta(1-D)T}\right)}{\beta DT\left(1-e^{\beta T}\right)}} \\ &= \sqrt{D}I_o\cdot\lambda \end{aligned} \tag{35}$$

$$\begin{aligned} I_{c,\rm rms} &= \sqrt{\frac{1}{T}\int_{nT}^{(n+1)T}\left[i_{c,\rm ss}^{n\rm th}\right]^2 dt} \\ &= \sqrt{D}I_o\sqrt{\left(\frac{R_b}{R_b+R_c}\right)^2\left[\frac{1}{\beta DT}\frac{e^{\beta DT}-e^{\beta T}-1+e^{\beta(1-D)T}}{1-e^{\beta T}}\right]} \\ &= \sqrt{D}I_o\cdot\mu \end{aligned} \tag{37}$$

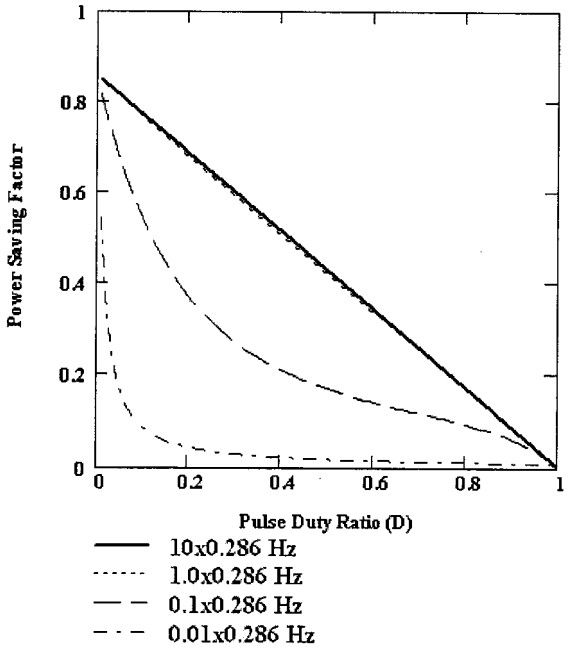

Fig. 7. Power saving factor as a function of the duty ratio for different pulse frequency. $m = 1$.

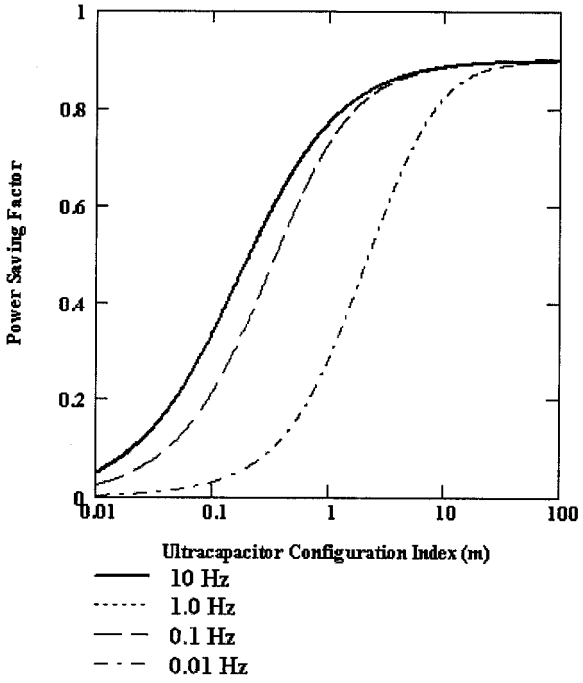

Fig. 8. Fractional power savings as a function of the index number for different pulse frequencies. $D = 0.1$.

square root in (37). The total internal loss for the battery–ultracapacitor system is

$$\begin{aligned} W_{i,\mathrm{bc}} &= \left(R_b I_{b,\mathrm{rms}}^2 + R_c I_{c,\mathrm{rms}}^2\right) \cdot \tau_{\mathrm{bc}} \\ &= R_b D I_o^2 \left(\lambda^2 + \frac{R_c}{R_b}\mu^2\right) \tau_{\mathrm{bc}} \\ &= R_b D I_o^2 \left(1-\varepsilon\right) \tau_{\mathrm{bc}} \end{aligned} \tag{38}$$

where τ_{bc} is the total run time for the battery–ultracapacitor system, and

$$\varepsilon = 1 - \left(\lambda^2 + \frac{R_c}{R_b}\mu^2\right). \tag{39}$$

Comparing (38) to (33), we see that

$$\varepsilon = 1 - \frac{R_b D I_o^2 \left(1-\varepsilon\right)}{R_b D I_o^2} = 1 - \frac{P_{i,\mathrm{bc}}}{P_{i,b}} = \frac{P_{i,b} - P_{i,\mathrm{bc}}}{P_{i,b}} \tag{40}$$

where $P_{i,\mathrm{bc}}$ is the internal power loss in the hybrid system, and $P_{i,b}$ is the internal power loss in the battery-alone system. ε is therefore interpreted as the fraction of the power normally lost in a battery powered system that is now saved by the hybrid system. Hereafter, we call this the power saving factor.

The power saving factor is shown in Fig. 7 as a function of the pulse duty ratio and pulse frequency. Power savings increase more completely at smaller duties. Savings approach 0 when $D \to 1$ because the utilization of the capacitor is zero for a DC current output. For all frequencies, the theoretical best power saving is achieved when $D \to 0$, as given by (41).

$$\varepsilon \underset{D\to 0}{\to} \frac{R_b}{R_b + R_c}. \tag{41}$$

Using the cell parameters $R_b = 0.15\ \Omega$ and $R_c = 0.025\ \Omega$ in (41), the best possible power saving is 85.7%. Obviously the capacitor with smallest series resistance provides the best power saving, and higher frequencies result in better savings. At $f = 10$ Hz (the solid line) or higher, the saving factor approaches a limit. The limit as a function of the duty ratio is given by (42), shown by the thicker line in the figure $(m = 1)$. (Of course at higher frequencies, a conventional decoupling capacitor can be used to reduce losses yet further. At these higher pulse frequencies the large capacity of the ultracapacitor is not needed.)

$$\varepsilon(D,m) \underset{f\to\infty}{\to} (1-D)\frac{R_b}{R_b + \frac{R_c}{m}}. \tag{42}$$

The effect of the ultracapacitor bank configuration on the power savings is shown in Fig. 8, where the power savings are graphed as a function of the configuration index m, with frequency as a parameter. Notice that the power savings increase as the number m increases. In the limit, 90% saving (for $D = 0.1$) may be achieved for an infinite number of capacitors. The figure also shows the positive effect of higher frequencies on the saving. When the operating frequency is higher than the maximum system eigen-frequency (2 Hz), the power savings approach a limit. In the figure, the thicker line for the pulse rate of 1 Hz is overlapped with the dotted line for 10 Hz, indicating they are already in the limit. The limit as a function of m is also given by (42).

C. Run Time Extension

The total energy saved under a parallel-connected battery–ultracapacitor system for a pulsed load current given by (5), according to (33) and (38), can be calculated as

$$\begin{aligned} \Delta W &= W_i - W_{i,\mathrm{bc}} = R_b D I_o^2 \tau_{\mathrm{bo}} - R_b D I_o^2 (1-\varepsilon)\tau_{\mathrm{bc}} \\ &= R_b D I_o^2 [\tau_{\mathrm{bo}} - (1-\varepsilon)\tau_{\mathrm{bc}}]. \end{aligned} \tag{43}$$

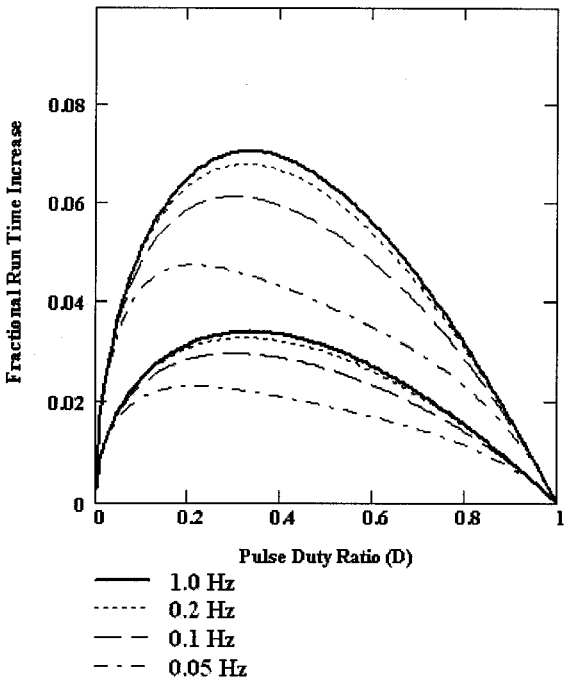

Fig. 9. Fractional increase of run time for the battery–ultracapacitor system as a function of the pulse duty ratio for different pulse frequencies. $m = 1$.

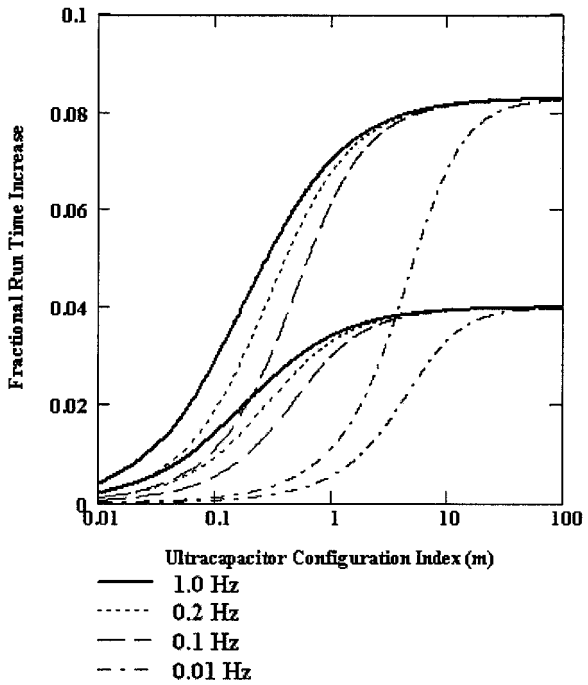

Fig. 10. Fractional increase of the run time as a function of the ultracapacitor bank configuration index m for different pulse frequencies.

Because energy is conserved, the run time is extended. The extension of the run time is

$$\Delta\tau = \frac{\Delta W}{P_o} \tag{44}$$

where P_o is the output power given by (45).

$$P_o = \frac{W_T - W_{i,\mathrm{bc}}}{\tau_{\mathrm{bc}}} = \frac{V_b\sqrt{D}I_o\tau_{\mathrm{bo}} - R_bDI_o^2(1-\varepsilon)\tau_{\mathrm{bc}}}{\tau_{\mathrm{bc}}}. \tag{45}$$

Using (43) and (45) in (44), with $\Delta\tau = \tau_{\mathrm{bc}} - \tau_{\mathrm{bo}}$ yields

$$\frac{\Delta\tau}{\tau_{\mathrm{bo}}} = \frac{\varepsilon\delta\sqrt{D}}{1-\varepsilon\delta\sqrt{D}}. \tag{46}$$

Equation (46) gives the fractional increase of the run time for the battery–ultracapacitor system compared to the battery-only system. There are three factors that influence the discharge life. Namely, the power saving factor ε, the duty ratio D and the ratio of the amplitude of the load current to the battery short-circuit current δ. The value of δ also indicates the percentage of the voltage drop across the internal resistance for the battery-alone system. When $\delta = 0$, the time extended is zero. Physically this is because there is no internal dissipation, therefore there is nothing to save for extending the run time. In the following discussion, we will choose δ as an independent parameter to see how the pulse duty, rate and capacitor configuration affect the run time extension.

The effect of the pulse rate and duty ratio can be viewed in Fig. 9 where (46) is plotted. There are two groups of curves. The upper group is for $\delta = 0.2$, and the lower one is for $\delta = 0.1$. As can be seen, higher frequencies result in better time extension. When the frequency is higher than the system eigen-frequency (0.286 Hz), the extension approaches the limits, indicated by the thicker lines in the figure. Notice that the line for 1 Hz already in the limit. Using (42) in (46), the expression for the limit can be found as

$$\frac{\Delta\tau}{\tau_{\mathrm{bo}}} \underset{f\to\infty}{\to} \frac{(1-D)\delta\sqrt{D}R_b}{\left(R_b + \frac{R_c}{m}\right) - (1-D)\delta\sqrt{D}R_b}. \tag{47}$$

The extension for the run time is zero when the duty approaches 1, since the power saving is nearly zero for a dc current. The extension is also zero when the duty approaches 0, although the power saving achieves its maximum. This is because a zero current output will not extend the run time anyway. The maximum run time extension occurs somewhere between the duty ratio 0 and 1. The position of the maximum extension depends also on the frequency and the current ratio δ. In the limit when the frequency is much higher than the system eigen-frequency, the position is independent of the device parameters and the current ratio, which can be found from (47) as

$$D_{\max} = \frac{1}{3}. \tag{48}$$

Fig. 10 shows the fractional increase in run time as a function of the ultracapacitor bank configuration index m under the same cell parameter conditions used previously and for $D = 0.3$. Since increasing m will decrease the system eigen-frequency, therefore the fractional run time monotonically increases as m increases. For any values of m, higher frequencies result in better run time increase. As long as the frequency is near or higher than the maximum eigen-frequency (2 Hz), the run time increase will approach the limits shown by the thick lines in Fig. 10 and described by (47). At 1 Hz (the thicker line also), they are already in the limits. Also shown are the dotted lines for 0.2 Hz, the dashed lines for 0.1 Hz, and the dot-dashed for 0.01 Hz. The lines approaching 0.083 for larger m correspond to $\delta = 0.2$, while the lines approaching 0.04 for large m correspond to $\delta = 0.1$. At best, the fractional run time increases are 8.3%

TABLE I
PARAMETER EFFECT ON SYSTEM PERFORMANCES

Performances	$m\uparrow$	$D\uparrow$	f$\uparrow$
Peak Power Enhancement Factor γ	↑	↓	↑
Power saving Factor ε	↑	↓	↑
Fractional Run Time Increase $\Delta\tau/\tau_{bo}$	↑	Max at $D=1/3$	↑

and 4%, respectively, for the current ratios of $\delta = 0.2$ and 0.1 when the duty ratio is 0.3. These values can also be calculated according to the (49), which is the maximum fractional run time increase that can be achieved, in general, when m is very large

$$\frac{\Delta\tau}{\tau_{\rm bo}} \underset{m\to\infty}{\to} \frac{(1-D)\delta\sqrt{D}}{1-(1-D)\delta\sqrt{D}}. \tag{49}$$

V. OPTIMIZATION

To optimize the system design, we categorize the parameters that influence the performance of the battery–ultracapacitor system into two groups: (1) the ultracapacitor bank configuration parameter m, and (2) the operating conditions, including the load current pulse duty ratio D and pulse frequency f. Since the operating conditions are dependent on the assumed known power demand of the load, we therefore optimize by seeking a best possible m value (related to the ultracapacitor size and configuration) under given D and f. To do so, the effects of these parameters on the peak power enhancement, the internal power loss reduction and the run time extension are summarized in Table I. The effects listed in the table are the results of increasing the values of the above three parameters.

As indicated by this table, within the tolerances of the load profile, it is preferable to choose higher values for f, while it is preferable to choose $D = 1/3$ for best system performance. In practice, the pulse rate and duty will be known properties of the load. They are generally not available as tunable design parameters. Increasing the value of m has a better effect on all three performances of the system. However, if you choose m, your choice must be made based on the system power level specifications which include a design of the highest power density and the highest possible efficiency. To do so, the following design procedures are suggested.

Given the load power requirement P, the load voltage (V_o) usually is given also, and from which the battery voltage can be decided $(V_b \approx V_o)$. Notice that in this simplified analysis, we assume the battery terminal voltage will closely match the load voltage. From the load profile (a pulsed load current), we then can determine the magnitude of the output current $(I_o = P/(\sqrt{D}V_o))$. If this is a battery-only system, the number of battery cells is

$$n_b = \frac{I_o}{I_{\rm rated}} = \gamma \tag{50}$$

where $I_{\rm rated}$ is the rated current of a single battery cell. Notice that (20) was used in (50), which says the peak power enhancement factor is equal to the number of battery cells for a given output current magnitude I_o. Instead of using multiple battery cells in parallel, an ultracapacitor bank will be used. The current shared by the ultracapacitor bank can be determined as

$$\zeta_c = 1 - \frac{1}{n_b} = 1 - \frac{1}{\gamma}. \tag{51}$$

Note that (51) is exactly the same as (19); although (51) is obtained purely from a practical design point of view. This illustrates that the previous theoretical analysis follows common sense. Equation (51) gives the ultracapacitor current sharing factor provided that the battery peak current is at the rated level. If, however, a lower battery current is considered for the sake of a longer lifetime, (50) can be modified as

$$n_b = \frac{I_o}{a \cdot I_{\rm rated}} \tag{52}$$

where $a < 1$ gives a fraction of the battery-rated current. Obviously, according to (51), a larger share in current for the ultracapacitor bank will result if (52) is used.

Next we will determine the value of m to complete the design by using (27) and (51). Because the current sharing factor is known, the minimum m value can be found by equating (27) to (51). This yields

$$1 - \frac{1}{n_b} = \frac{R_b e^{-\beta(m)DT}}{R_b + \frac{R_c}{m}} \frac{1 - e^{-\beta(m)(1-D)T}}{1 - e^{-\beta(m)T}}. \tag{53}$$

Equation (53) can be graphically solved, as shown in Fig. 11. The curves shown in the figure are the current sharing factors of the ultracapacitor bank as functions of m, D and f, which are represented by the right hand side of (53). The solid, the dotted, the dashed and the dot-dashed curves are for the frequencies of 10, 1, 0.1, and 0.02 Hz, respectively. The duty ratio is chosen at value of 0.1 in the calculation. The horizontal lines are the current sharing factors as a function of the peak power enhancement factor, which are represented by the left-hand side of the (53). The solid, the dotted, the dashed and the dot-dashed

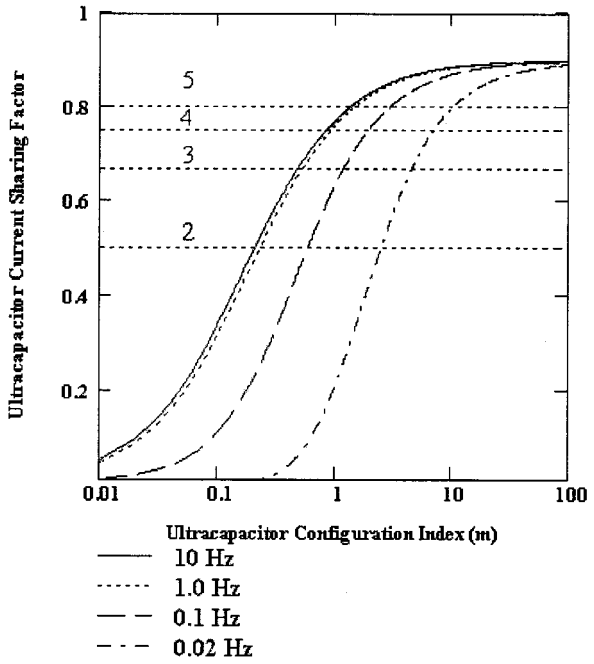

Fig. 11. Solutions to (53) are the intercepts of the curves with horizontal lines.

TABLE II
DATA FOR BATTERY AND ULTRACAPACITOR

Device	Capacity	Voltage (V)	ESR (Ω)	Size (mm)	Weight (g)
Sony LIP2000	1.35 Ahr	7.2	(0.3)	38.5x70.7x20.5	100
Maxwell PC10	10 F	2.5	0.15 (DC)	24x31x4.5	6

TABLE III
COMPARISON OF OPTIMIZED HYBRID TO BATTERY-ALONE SYSTEM

Systems	Peak Power (W)	Loss (W)	Discharge time (hr)	Volume (cm^3)	Weight (g)
Single Battery	36 (risk)	0.75	2.7	55.8	100
5 Batteries	36	0.15	13.5	167.4	500
1Battery/3x7 PC10 Cells	36	0.20	2.84	126.1	226

straight lines are for the peak power enhancement factors of 2, 3, 4, and 5, respectively. The solutions are the intersections of these lines and curves. If the peak power enhancement factor is 4, the LHS of (53) yields a current sharing factor of 0.75 (75% of the total current). Checking the intercepts of the dashed straight line with the curves, it can be found that the m value for the frequencies of 10, 1, 0.1, and 0.02 Hz are 0.84, 0.92, 1.92, and 6.9.

The solution to (53) simply gives a minimum value of m for the load power requirement with highest possible power density. A larger m value will increase the system performance, but at a cost to the system price, volume, and weight. Since noninteger values were found, the larger but closest values will be chosen. For example, we choose $m = 1$, 1, 2, and 7 for the power enhancement factor of 2, 3, 4, and 5, respectively. At this point, the results of optimization are obvious. For example, instead of having four cells of the batteries to satisfy the load requirement, it can be achieved with one cell of the battery in parallel with 1 cell of the ultracapacitors operated at a frequency at least 1 Hz, or with two cells of ultracapacitors operated at a frequency at least 0.1 Hz. Obviously, for very low frequencies, there are no advantages to take since the volume of the capacitor would have to be large to achieve the same goal. But at higher frequencies, the system volume and weight can be greatly reduced.

VI. DESIGN EXAMPLE

To illustrate the application of the optimization, let's consider a design example by using the above results. The data of a typical Li-Ion-Polymer battery and an ultracapacitor are given in Table II. The resistance of the battery in the table is obtained through the curve fitting of the discharge characteristics, since it is not available in the manufacturer's data sheet. Note that the batteries of Li-Ion types receive great attention recently in advanced power system applications due to its high voltage, light weight and high energy density. Our goal is to design an optimized battery–ultracapacitor system for best possible system performances.

Since the rated voltage for capacitors is 2.5 V, three cells of PC10 will be used in series. Therefore $n_s = 3$. The resulting voltage for the capacitor is 7.5 V, which is safely enough above the battery terminal voltage. The device parameters are: $R_c = 0.15\ \Omega$, $C_c = 10$ F, $R_b = 0.3\ \Omega$, $V_b = 7.2$ V.

Assuming the load current has the following parameters: $D = 0.1$, $f = 1$ Hz, and amplitude $I_o = 5$ A. The power required by the load is

$$P_o = \sqrt{D} I_o V_b = 11.4\,(\text{W}).$$

If the battery allows to run 5 A, the power loss will be

$$P_{i,b} = R_b D I_o^2 = 0.75\ (\text{W}).$$

The total discharge time, assuming the battery can discharge 100% at 7.2 V, is

$$\tau_{\text{bo}} = \frac{1.35}{D I_o} = 2.7\,(\text{hr}).$$

However, not only can this discharge time not be guaranteed, but also it risks the battery's safety, since the operating current is far beyond the manufacturer suggested limits. If 5 batteries are used instead, we know that the system volume and weight will be five times higher.

To design an ultracapacitor bank, we first notice that the power enhancement factor (50) is

$$\gamma = \frac{5}{1.35} = 3.7.$$

This yields the capacitor current sharing factor of 0.73. Using the enhancement factor value, the device parameters, and the pulse parameters in (53), it can be found that $m = 2.2$. Equation (23) results in $n_p = n_s \cdot m = 6.6 \approx 7$. Therefore, there will be total 3×7 PC10 cells for the bank. The system eigen-frequency, according to (24), is $\beta = 0.118$, which is much smaller than the pulse frequency (1 Hz). It can be expected that, based on the previous analysis, the system performance can be enhanced with the highest power density. The power loss saving is 74% according to (42), and the extension of the run time, estimated by (47), is 8.4 min. The results are listed in Table III.

VII. CONCLUSION

We have analytically demonstrated that a battery–ultracapacitor hybrid power source can supply a pulsed load with higher peak power, smaller internal losses and greater discharge life of the battery, than can the battery-powered system alone. The details of the peak power enhancement, loss reduction and run time extension were discussed in terms of the load profile parameters such as the pulse duty ratio, the pulse rate, and the ultracapacitor bank size and configuration. The results can be used to optimize a system design. An example of the capacitor bank configuration optimization was illustrated. Currently, we are focusing on more accurate characterization of runtime improvements and loss reduction via simulation, using highly detailed models of the battery and capacitor components.

APPENDIX

A. Battery Peak Current

All proceeding terms contribute to the maximum current of the nth pulse at $t=(n+D)T$. According to (15):

$$\begin{aligned} I_{b,\text{peak}} =& i_{b,\text{ss}}[(n+D)T] \\ =& I_o \sum_{k=0}^{n} \Bigg[\left(1-\frac{R_b}{R_b+R_c}e^{-\beta(n+D-k)T}\right) \\ & \times \Phi[(n+D-k)T] \\ & - \left(1-\frac{R_b}{R_b+R_c}e^{-\beta(n-k)T}\right) \\ & \times \Phi[(n-k)T] \Bigg]. \end{aligned} \tag{A1}$$

Since step functions $\Phi[(n+D-k)T]$ and $\Phi[(n-k)T]$ are equal to 1 at $t=(n+D)T$, also notice that the second term is zero when $k=n$, we therefore have

$$\begin{aligned} I_{b,\text{peak}} =& I_o \Bigg\{ \sum_{k=0}^{n-1} \Bigg[\left(1-\frac{R_b}{R_b+R_c}e^{-\beta(n+D-k)T}\right) \\ & - \left(1-\frac{R_b}{R_b+R_c}e^{-\beta(n-k)T}\right) \Bigg] \\ & + 1-\frac{R_b}{R_b+R_c}e^{-\beta DT} \Bigg\} \\ =& I_o \Bigg\{ 1-\frac{R_b}{R_b+R_c}e^{-\beta DT}+\frac{R_b}{R_b+R_c}e^{-n\beta T} \\ & \times \left(1-e^{-\beta DT}\right) \sum_{k=0}^{n-1} \left[e^{k\beta T}\right] \Bigg\} \\ =& I_o \Bigg\{ 1-\frac{R_b}{R_b+R_c}e^{-\beta DT}+\frac{R_b}{R_b+R_c}\left(1-e^{-\beta DT}\right) \\ & \times \left(\frac{e^{-n\beta T}-1}{1-e^{\beta T}}\right) \Bigg\} \\ \underset{n\to\infty}{\rightarrow}& I_o \left[1-\frac{R_b}{R_b+R_c}\frac{e^{-\beta DT}\left(1-e^{-\beta(1-D)T}\right)}{1-e^{-\beta T}}\right]. \end{aligned} \tag{A2}$$

This is (17).

B. Root-Mean-Square Currents

Consider nth battery current pulse only. From (34), it can be derived

$$\begin{aligned} i_{b,\text{ss}}^{n\text{th}} =& I_o \Bigg[1+\frac{R_b}{R_b+R_c} \\ & \times e^{-\beta t}\left(\frac{(e^{\beta DT}-1)(1-e^{n\beta T})}{1-e^{\beta T}}-e^{n\beta T}\right)\Bigg] \\ & \times [\Phi[t-nT]-\Phi[t-(n+1)T]] \\ & - I_o \left[1-\frac{R_b}{R_b+R_c}e^{-\beta[t-(n+D)T]}\right] \\ & \times [\Phi[t-(n+D)T]-\Phi[t-(n+1)T]]. \end{aligned} \tag{A3}$$

Integrating the square of the above expression from nT to $(n+1)T$, the result is

$$\begin{aligned} & \int_{nT}^{(n+1)T} \left(i_{b,\text{ss}}^{n\text{th}}\right)^2 dt \\ & = I_o^2 \Bigg[DT+\frac{R_b}{R_b+R_c}\frac{2(1-e^{-\beta DT})}{\beta}\left(\frac{1-e^{\beta DT}}{1-e^{\beta T}}-1\right) \\ & \quad + \left(\frac{R_b}{R_b+R_c}\right)^2 \frac{(e^{\beta DT}-1)(1-e^{\beta(1-D)T})}{\beta(1-e^{\beta T})} \Bigg]. \end{aligned} \tag{A4}$$

Divide the above expression by T and take a square root operation, (35) can be obtained. Equation (37) can be derived in a similar way.

REFERENCES

[1] A. Yoshida, K. Imoto, H. Yodeda, and A. Nishino, "An electric double-layer capacitor with high capacitance and low resistance," *IEEE Trans. Comp., Hybrid, Manufact. Tech.*, vol. 15, pp. 133–138, Feb. 1992.

[2] A. F. Burke and J. R. Miller, "Test procedures for high energy density, electrochemical capacitors," in *Proc. Electrochem. Soc. Conf.*, vol. 95-29, 1995, pp. 280–297.

[3] B. E. Conway, *Electrochemical Supercapacitors: Scientific Fundamentals and Technological Applications*. New York: Kluwer-Plenum, 1999.

[4] R. Kötz and M. Carlen, "Principles and applications of electrochemical capacitors," *Electrochem. Acta*, vol. 45, pp. 2483–2498, 2000.

[5] S. M. Halpin, R. L. Spyker, R. M. Nelms, and R. F. Burch, "Application of double-layer capacitor technology to static condensers for distributed system voltage control," *IEEE Trans. Power Syst.*, vol. 11, pp. 1899–1904, Nov. 1996.

[6] K. Harada, E. Sakai, H. Hyakutake, G. Ariyoshi, and K. Yamasaki, "Power system with cold stand-by using ultra capacitors," in *Proc. 12th Int. Telecommun. Energy Conf. (INTELEC'98)*, 1998.

[7] P. Pillay, R. M. Samudio, M. Ahmed, and R. T. Patel, "A chopper-controlled SRM drive for reduced acoustic noise and improved ride-through capability using supercapacitors," *IEEE Trans. Ind. Applicat.*, vol. 31, pp. 1029–1037, Sept./Oct. 1995.

[8] R. L. Spyker and R. M. Nelms, "Optimization of double-layer capacitor arrays," *IEEE Trans. Ind. Applicat.*, vol. 36, pp. 194–198, Jan./Feb. 2000.

[9] L. Zubieta and R. Bonert, "Characterization of double-layer capacitors for power electronics applications," *IEEE Trans. Ind. Applicat.*, vol. 36, pp. 199–204, Jan./Feb. 2000.

[10] J. R. Miller, "Battery–capacitor power source for digital communication applications: Simulations using advanced electrochemical capacitors," in *Proc. Electrochem. Soc. Conf.*, vol. 95-29, Oct. 1995, pp. 246–254.

[11] L. P. Jarvis, T. B. Atwater, and P. J. Cygan, "Fuel cell/electrochemical capacitor hybrid for intermittent high power applications," *J. Power Sources*, vol. 79, pp. 60–63, 1999.

[12] T. B. Atwater, P. J. Cygan, and F. C. Leung, "Man portable power needs of the 21st century I. Applications for the dismounted soldier. II. Enhanced capabilities through the use of hybrid power sources," *J. Power Sources*, vol. 91, pp. 27–36, 2000.

[13] L. P. Jarvis, T. B. Atwater, and P. J. Cygan, "Hybrid power sources for land warrior scenario," *IEEE Aerosp. Electron. Syst. Mag.*, pp. 37–41, Sept. 2000.

[14] P. J. Mahon, G. L. Paul, S. M. Keshishian, and A. M. Vassallo, "Measurement and modeling of the high-power performance of carbon-based supercapacitors," *J. Power Sources*, vol. 91, pp. 68–76, 2000.

R. A. Dougal (SM'94) received the B.S., M.S., and Ph.D. degrees from Texas Tech University, Lubbock, in 1978, 1980, and 1983, respectively, all in electrical engineering.

He is Director of the Virtual Test Bed project, a multidisciplinary, multiuniversity effort to develop a comprehensive simulation and virtual prototyping environment for advanced power systems, integrating power electronics, electromechanics, electrochemistry, and controls into a common testbed. The VTB is unique in allowing the simulation of multidisciplinary systems by importing models from discipline specific source languages to a common workspace. In addition to modeling and simulation, his expertise includes power electronics, physical electronics, and plasmas.

Shengyi Liu (M'95) received the B.Sc. and M.Sc. degrees from Tsinghua University, Beijing, China, in 1982 and 1985, respectively, and the Ph.D. degree in electrical engineering from the University of South Carolina, Columbia, in 1995.

Prior to joining the Department of Electrical Engineering, University of South Carolina, as a Research Professor, he was Senior Research and Development Engineer, from 1995 to 1999, at InnerLogic, Inc. Research interests include application and control study of advanced power sources and systems, and modeling and simulation of interdisciplinary systems under virtual test bed computational environment. His interests also include modeling, design, and applications of physical electronics-based devices, power semiconductor devices, and converters.

Ralph E. White received the Ph.D. degree from the University of California, Berkeley, in 1977.

He was faculty at Texas A&M University, College Station, from 1977 to 1993, then moved to the University of South Carolina, Columbia, as Westinghouse Distinguished Scientist and Chairman of the Department of Chemical Engineering. He is currently the Dean of Engineering. He has published over 226 refereed journal articles and edited or co-edited over 36 books on electrochemistry.

Dr. White received research awards from the Battery Division and the Electrodeposition Division of The Electrochemical Society, and the 1999 Scientific Achievement Award from the American Electroplaters and Surface Finishing Society. He is a Fellow of The Electrochemical Society